

Temperature Scalings and Profiles in Forced Convection Turbulent Boundary Layers

Xia Wang¹

Department of Mechanical Engineering,
Oakland University,
Rochester, MI 48309
e-mail: wang@oakland.edu

Luciano Castillo

Guillermo Araya

Department of Mechanical Engineering,
Aerospace and Nuclear Engineering,
Rensselaer Polytechnic Institute,
Troy, NY 12180

Based on the theory of similarity analysis and the analogy between momentum and energy transport equations, the temperature scalings have been derived for forced convection turbulent boundary layers. These scalings are shown to be able to remove the effects of Reynolds number and the pressure gradient on the temperature profile. Furthermore, using the near-asymptotic method and the scalings from the similarity analysis, a power law solution is obtained for the temperature profile in the overlap region. Subsequently, a composite temperature profile is found by further introducing the functions in the wake region and in the near-the-wall region. The proposed composite temperature profile can describe the entire boundary layer from the wall all the way to the outer edge of the turbulent boundary layer at finite Re number. The experimental data and direct numerical simulation (DNS) data with zero pressure gradient and adverse pressure gradient are used to confirm the accuracy of the scalings and the proposed composite temperature profiles. Comparison with the theoretical profiles by Kader (1981, "Temperature and Concentration Profiles in Fully Turbulent Boundary Layers," *Int. J. Heat Mass Transfer*, **24**, pp. 1541–1544; 1991, "Heat and Mass Transfer in Pressure-Gradient Boundary Layers," *Int. J. Heat Mass Transfer*, **34**, pp. 2837–2857) shows that the current theory yields a higher accuracy. The error in the mean temperature profile is within 5% when the present theory is compared to the experimental data. Meanwhile, the Stanton number is calculated using the energy and momentum integral equations and the newly proposed composite temperature profile. The calculated Stanton number is consistent with previous experimental results and the DNS data, and the error of the present prediction is less than 5%. In addition, the growth of the thermal boundary layer is obtained from the theory and the average error is less than 5% for the range of Reynolds numbers between 5×10^5 and 5×10^6 when compared with the empirical correlation for the experimental data of isothermal boundary layer conditions.

[DOI: 10.1115/1.2813781]

Keywords: turbulent boundary layer, similarity analysis, forced convection heat transfer, temperature scaling

1 Introduction

Heat transfer in turbulent boundary layers has attracted many researchers due to its various applications in industry such as in heat exchangers, gas turbine blades, aircrafts, electronic cooling, and so on. However, this phenomenon remains unsolved due to the complexity of nonlinear turbulent quantities. The problem of forced convection turbulent boundary layer flow is worse in the case of pressure gradient flows, particularly in adverse pressure gradient (APG) flow.

Experimental investigations related to forced convection turbulent boundary layers were mainly performed during and before the 1970s. Analytical studies and numerical simulations have been the main tool to investigate heat transfer problems in boundary layer flows. Due to high computing cost and limitation of low Reynolds number flows, many complex flows in engineering applications are not well understood by numerical simulations alone, Gad-el-hak [1]. Therefore, dimensional analysis and similarity analysis are still useful tools in understanding the basic physics of heat transfer in turbulent boundary flows including high Reynolds number problems. Using dimensional analysis, Perry et al. [2]

investigated the velocity and temperature profiles in turbulent boundary layers subject to the APG. A half-power law was found for the velocity profile and an inverse-half-power law for the temperature profile in the region of the pressure gradient layer. Furthermore, Afzal [3] derived the same power law using the matched asymptotic expansion method. These power laws were limited to describe the temperature profile in a small overlap region and cannot be used to describe the entire boundary layer. Kader [4] later proposed the following equations to describe the temperature profile in the zero pressure gradient (ZPG) turbulent boundary layers as

$$\frac{T_w - T}{T_r} = P_r y^+ \exp(-\Gamma) + \left\{ 2.12 \ln \left[(1 + y^+) \frac{2.5(2 - \bar{y})}{1 + 4(1 - \bar{y})^2} \right] + \beta(P_r) \right\} \exp\left(-\frac{1}{\Gamma}\right) \quad (1)$$

where $y^+ = yu_\tau/\nu$, $\bar{y} = y/\delta$, $\Gamma = 10^{-2}(P_r y^+)^4/(1 + 5P_r^3 y^+)$, and $\beta(P_r) = (3.85P_r^{1/3} - 1.3)^2 + 2.12 \ln P_r$. This equation was derived assuming that a single temperature scaling exists in the overlap region. A decade later, Kader [5] investigated the temperature profile of turbulent boundary layer flow subject to pressure gradient using dimensional analysis and the asymptotic method. The boundary layer was divided into three regions, and each region was described by a given formulation. Moreover, these equations were derived based on the assumption of a moving-equilibrium bound-

¹Corresponding author.

Contributed by the Heat Transfer Division of ASME for publication in the *JOURNAL OF HEAT TRANSFER*. Manuscript received June 13, 2006; final manuscript received May 30, 2007; published online February 4, 2008. Review conducted by Anthony M. Jacobi.

ary layer, which means that for a given value of the streamwise location x , all the characteristics of the fluid flow depend on the local value of the position of x only. However, recent investigators argued that the downstream flow cannot forget its upstream history, and the upstream conditions, such as the tripping wire (its shape, size, and location) and the wind tunnel speed will have some effects on the development of the downstream flow, Erm and Joubert [6], Castillo and Johansson [7], and Castillo and Walker [8].

Instead of using conventional dimensionless analysis or similarity analysis, Churchill et al. [9,10] proposed an algebraic model to scale the mean turbulence quantities, turbulence Reynolds stresses, and turbulence heat flux. Le and Papavassiliou [11] used the theory of Churchill et al. [9,10] to develop a temperature profile for low Re turbulent flow. Moreover, Wei et al. [12,13] developed the so-called "multiscale analysis" in order to study the structure of the turbulent boundary layer with and without heat transfer. Different from all the previous studies, George and co-workers introduced the near-asymptotic method [14,15]. George [14] used a near-asymptotic method in order to derive the solution of the velocity profile in the overlap region. By matching the profiles in the inner and outer regions at the finite Re number, a velocity profile can be obtained. This approach is opposite to the classical method in which the velocity profiles are obtained in the limit of infinite Reynolds number. Using the near-asymptotic method, George and Castillo [15] derived a power law solution for the velocity profile in the overlap region of a ZPG turbulent boundary layer. They further proposed a composite velocity profile for the same type of flow. George et al. [16] discussed that a power law solution should also exist to describe the temperature profile in the overlap region of a thermal boundary layer. In the current investigation, the temperature scaling derived by Wang and Castillo [17] will be reviewed first. Then using the new temperature scalings proposed by Wang and Castillo [17], a new power law solution will be derived for the temperature profile in the overlap region by applying the near-asymptotic theory. Furthermore, a composite temperature profile is constructed by introducing a new wake function for the outer region and a function describing the near-wall region. In addition, this composite temperature profile will be verified using the ZPG and APG experimental data of Blackwell [18], Reynolds [19] and the direct numerical simulation (DNS) data of Kong et al. [20]. Also, the theoretical profiles of Kader [4,5] will be used for comparison and verification of the present theory. A unique feature of the proposed new composite temperature profile is its validity at the finite Re number over the entire thermal boundary layer (i.e., from the near-the-wall region to the outer region). In addition, this new composite temperature profile will be applied to the energy integral equation to calculate the heat transfer law.

2 Theory

2.1 Temperature Scalings From Similarity Analysis. In the limit as the Reynolds number goes to the infinity, the boundary layer equations become independent of the Reynolds number, Schlichting and Gersten [21], George and Castillo [15]. Therefore, any scaling or function representing the boundary layer solutions must also be independent of the Reynolds number in this limit. Consequently, the inner and outer scalings of turbulent boundary layers can also be determined in this limit (i.e., the asymptotic invariance principle: AIP proposed by George and Castillo [15]). Most recently, Wang and Castillo [17] applied this theory to forced convection turbulent boundary layers with and without external pressure gradient. Two different scalings are derived for the inner and outer regions, respectively. The temperature profiles can be written in inner and outer variables and given as

$$\frac{T_w - T}{T_{si}} = g_{si}(y_T^+; \delta_T^+) \quad (2)$$

$$\frac{T - T_\infty}{T_{so}} = g_{so}(\bar{y}_T; \delta_T^+) \quad (3)$$

Substituting Eqs. (2) and (3) into the inner and outer thermal turbulent boundary layers in the limit as $\delta_T^+ \rightarrow \infty$, the new inner and outer temperature scalings are found to be

$$T_{si} = \text{Pr} \sqrt{\text{St}} (T_w - T_\infty) \quad (4)$$

$$T_{so} = \frac{\delta_T^*}{\delta_T} (T_w - T_\infty) \quad (5)$$

The variables y_T^+ and \bar{y}_T are the inner and outer similarity length scales, respectively, defined as

$$y_T^+ = \frac{y U_\infty}{\nu} \sqrt{\text{St}} \quad (6)$$

$$\bar{y}_T = \frac{y}{\delta_T} \quad (7)$$

The ratio of inner to outer similarity length scales is denoted by δ_T^+ and given as

$$\delta_T^+ = \frac{y_T^+}{\bar{y}_T} = \frac{\delta_T U_\infty}{\nu} \sqrt{\text{St}} \quad (8)$$

The outer temperature scaling T_{so} includes the term δ_T^*/δ_T , which is the ratio of the thermal displacement thickness δ_T^* to the thermal boundary layer thickness δ_T . The thermal displacement thickness δ_T^* is defined as

$$\delta_T^* = \int_0^\infty \frac{T - T_\infty}{T_w - T_\infty} dy \quad (9)$$

Figures 2 and 3 show the comparison between the classical scaling and the new scaling using the ZPG and APG forced convection experimental data by Blackwell [18]. The APG experiments were performed in such a way that a power law relationship between the free stream velocity U_∞ and the streamwise distance x exists, i.e., $U_\infty \sim x^m$, where the power law coefficient m represents the strength of the pressure gradient. A different value of m means that the flow is subject to different strengths of the pressure gradient. The ZPG data are also from the experiment by Blackwell [18]. The Reynolds number based on θ varies between 515 and 2805 and the upstream wind tunnel speed is given by $U_o \approx 10$ m/s.

In the classical scaling, both the inner and outer temperature profiles were scaled with $T_\tau = q_w / \rho C p u_\tau$ where q_w is the heat flux imposed at the wall and u_τ is the friction velocity. For example, Fig. 2(a) shows various ZPG and APG experimental data in classical variables (i.e., T_τ and U_τ). Clearly, the profiles do not collapse into a single curve as one may expect in the classical view. For the experimental data with different strengths of the pressure gradient, the profiles collapse into a single curve for a given external strength of the pressure gradient; however, the collapsed profiles show different shapes as the pressure gradient changes. In contrast, the temperature profiles dimensionalized by the new scaling $T_{si} = \text{Pr} (T_w - T_\infty) \text{St}^{1/2}$ show an excellent collapse over the entire boundary layer as presented in Fig. 2(b). Notice that all the experimental data with different Reynolds numbers and pressure gradients collapse into the same curve, especially in the near-the-wall region. Thus, the new scaling is able to capture the influences of the local heat transfer and the external pressure gradient. This fact will be shown later to play a crucial role in determining the functional forms of the temperature profiles g_{si} and g_{so} .

Figures 3(a) and 3(b) show the same experimental data plotted in outer variables. Figure 3(a) shows the temperature profiles normalized by the friction temperature T_τ as given by the classical approach. Notice that for the experimental data with fixed up-

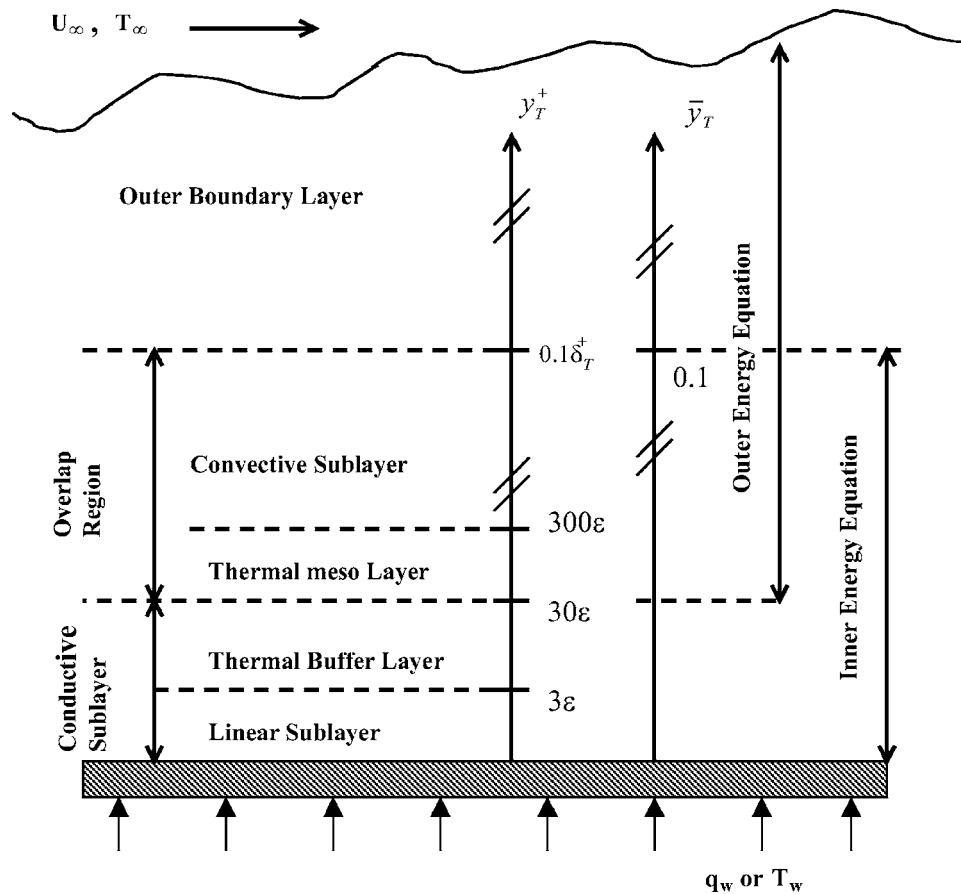


Fig. 1 Schematic showing various regions inside the thermal boundary layer

stream conditions and pressure gradient, the profiles collapse into one single curve. However, each of these profiles has different shapes from each other due to different external pressure gradients imposed on the flow. On the other hand, Fig. 3(b) shows the same experimental data using the new outer scaling $T_{so} = \delta_T^* \delta_T^* (T_w - T_\infty)$. Clearly, the new scaling, compared to the classical scaling, removes all the effects of pressure gradient and the dependence on the Reynolds number given by δ_T^* in the outer flow. Therefore, all profiles collapse into a single curve regardless of these effects.

Consequently, Figs. 2(b) and 3(b) indicate that an asymptotic temperature profile exists when the profiles are scaled by the new inner and outer scalings. Nevertheless, there may be a weak dependence in the overlap region on the Reynolds number.

2.2 Temperature Profiles in the Overlap Region. Proper temperature scalings have been reviewed in the previous section; these scalings are able to remove most of the effects from the Reynolds number dependence and different strengths of pressure gradients. In this section, an analytical function will be derived to describe the entire temperature profile from the near-the-wall region up to the outer region of the boundary layer.

The inner and outer temperature scalings will be used in order to determine the functional dependence in the overlap region (i.e., the common region between the inner and outer flows given in Fig. 1). Figure 1 shows the diagram of different layers within the thermal boundary layer, which corresponds to various regions within the velocity layer discussed by George and Castillo [15]. According to George and Castillo [15], an overlap region is found for the velocity boundary layer within the range of $30 < y^+ < 0.1\delta^+$. For the thermal boundary layer, an overlap region can be similarly transformed from the velocity overlap region as $30\epsilon < y_T^+ < 0.1\delta_T^+\epsilon$ considering $y_T^+ = y^+\epsilon$, where $\epsilon = \sqrt{St/(C_f/2)}$. The

overlap region includes two sublayers: one is the convective sublayer where the conduction term has almost no effect; the other one is the thermal mesolayer where the conduction term is not negligible, and it has certain effects on the turbulent heat flux term. The temperature scalings and the functions for the inner and outer flows will be employed together in order to build the composite temperature.

George and Castillo [15] proposed the near-asymptotic method to investigate the velocity profile in the ZPG boundary layer flow. This theory will be applied for the temperature profile in the overlap region of turbulent boundary layers. According to the near-asymptotic theory, the following conditions or assumptions should be satisfied. First, at the finite Re number given by δ_T^* , the temperature profile scaled in either inner or outer variables can describe the flow everywhere inside the boundary layer. Therefore, at finite Reynolds number, the inner temperature profile of Eq. (2) and the outer temperature profile of Eq. (3) must match each other, and it follows that

$$Q_T(\delta_T^+) = P_T(\delta_T^+)g_{si} + g_{so} \quad (10)$$

where

$$Q_T(\delta_T^+) = \frac{T_w - T_\infty}{T_{so}} \quad P_T(\delta_T^+) = \frac{T_{si}}{T_{so}} \quad (11)$$

for all values of y and δ_T^* . Second, the temperature derivatives with respect to the vertical position y should also be the same whether the temperature profile is expressed in terms of inner variables or outer variables at finite Re number. Consequently, for the fixed Re number given by δ_T^* , the temperature derivatives must match each other between the inner and outer regions, and it follows that

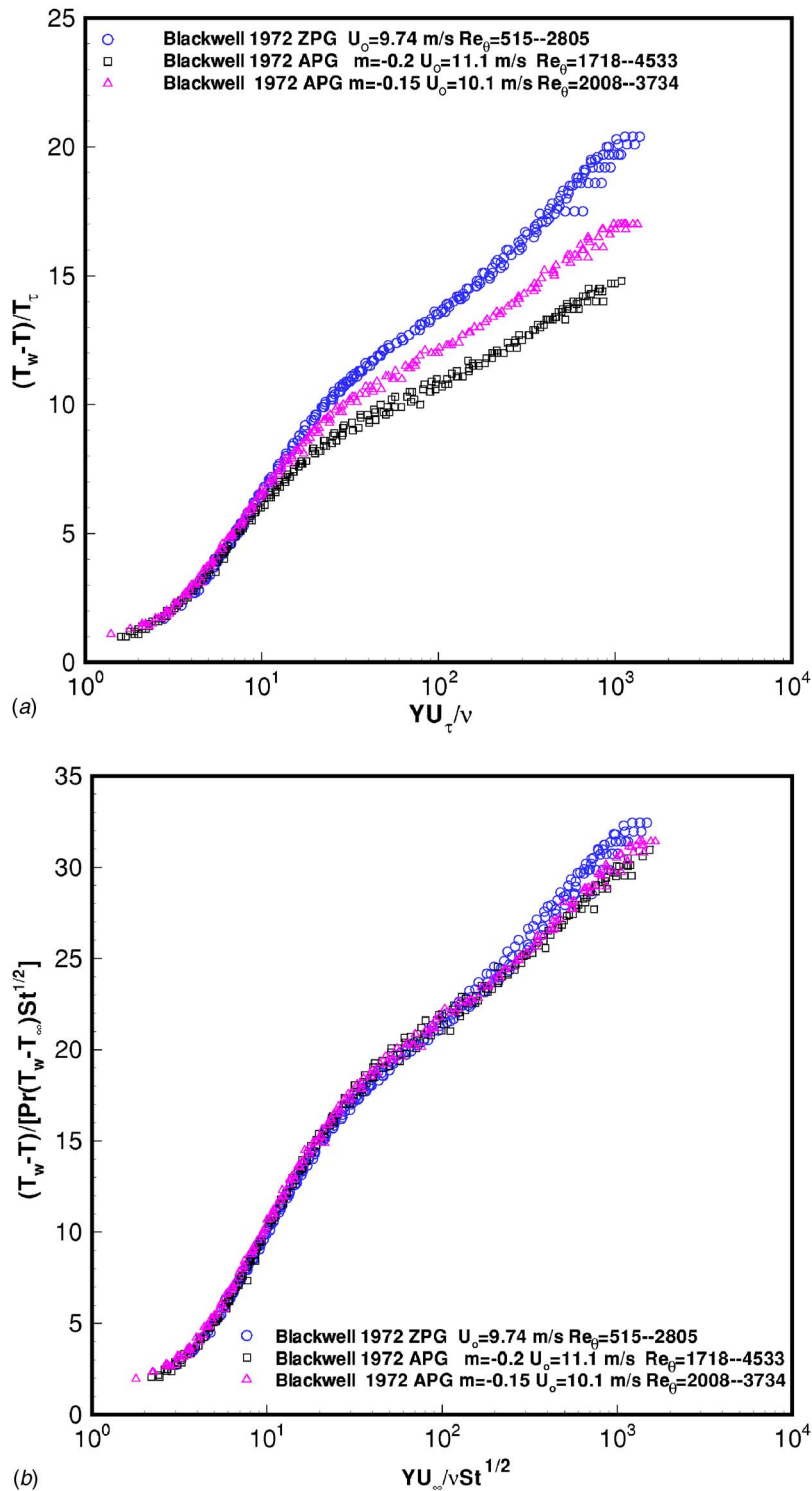


Fig. 2 Comparisons of the temperature profiles in inner variables using the classical scaling and present scaling for ZPG and APG flows

$$\bar{y}_T \left. \frac{\partial g_{so}}{\partial \bar{y}_T} \right|_{\delta_T^+} = -P_T(\delta_T^+) y_T^+ \left. \frac{\partial g_{si}}{\partial y_T^+} \right|_{\delta_T^+} \quad (12)$$

Since the overlap region cannot be maintained in a certain vertical position with the change of the downstream position x due to the fact that the boundary layer continues to grow in this direction, an intermediate variable \tilde{y}_T is introduced. This intermediate variable \tilde{y}_T can be fixed in the overlap region all the way to the limit of

$Re \rightarrow \infty$, regardless of what is happening in the physical space according to George and Castillo [15]. Using this intermediate variable \tilde{y}_T , the inner and outer length scales should take the following forms;

$$y_T^+ = \tilde{y}_T \delta_T^{+n} \quad \bar{y}_T = \tilde{y}_T \delta_T^{+n-1} \quad (13)$$

where $0 < n < 1$. In the limit as $\delta_T^+ \rightarrow \infty$, $\bar{y}_T \rightarrow 0$ and $y_T^+ \rightarrow \infty$ while \tilde{y}_T remains fixed in the overlap region along the boundary layer.

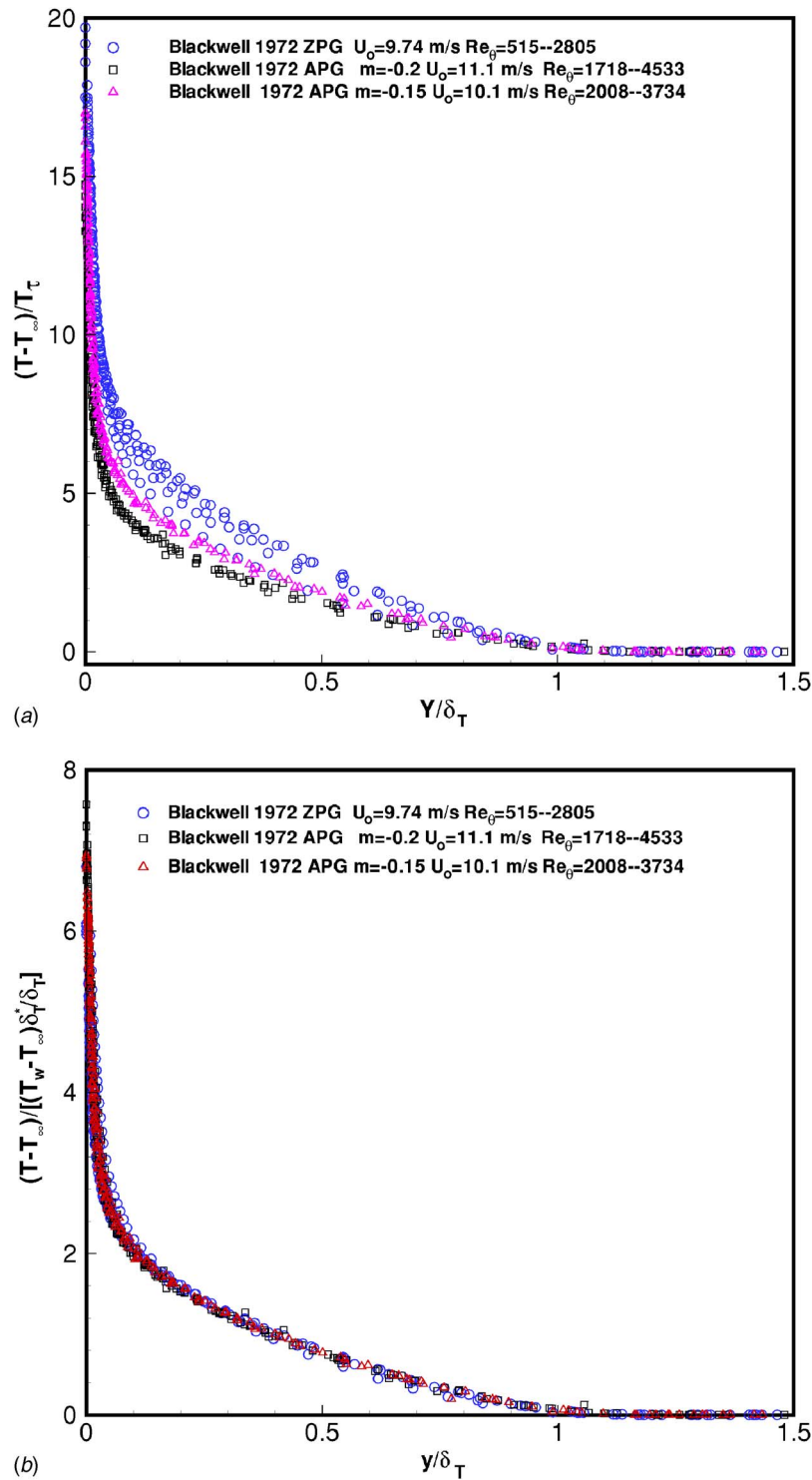


Fig. 3 Comparisons of the temperature profiles in outer variables using the classical scaling and present scaling for ZPG and APG flows

Therefore, the matching condition of Eq. (10) can be transformed in terms of the intermediate variable \bar{y}_T and given by

$$Q_T(\delta_T^+) = P_T(\delta_T^+) g_{si}(\bar{y}_T \delta_T^+; \delta_T^+) + g_{so}(\bar{y}_T \delta_T^{n-1}; \delta_T^+) \quad (14)$$

where the variables P_T and Q_T have the same definitions as given by Eq. (11). Differentiating Eq. (14) with respect to δ_T^+ for the fixed \bar{y}_T yields

$$\begin{aligned} \frac{dQ_T}{d\delta_T^+} \Big|_{\bar{y}_T} &= \frac{dP_T}{d\delta_T^+} g_{si} + P_T \left[\frac{\partial g_{si}}{\partial y_T^+} \Big|_{\delta_T^+} n \bar{y}_T \delta_T^{n+1} + \frac{\partial g_{si}}{\partial \delta_T^+} \Big|_{y_T^+} \right] \\ &+ \frac{\partial g_{so}}{\partial \bar{y}_T} \Big|_{\delta_T^+} (n-1) \bar{y}_T \delta_T^{n-2} + \frac{\partial g_{so}}{\partial \delta_T^+} \Big|_{\bar{y}_T} \end{aligned} \quad (15)$$

and clearing terms by using Eqs. (10) and (12)–(14), it follows that

$$\bar{y}_T \left. \frac{\partial g_{so}}{\partial \bar{y}_T} \right|_{\delta_T^+} = g_{so} \gamma_T + \phi_T + g_{so} \left(S_{oT} - S_{iT} + \frac{Q_T}{g_{so}} S_{iT} \right) \quad (16)$$

where

$$\gamma_T(\delta_T^+) = - \frac{\delta_T^+}{P_T(\delta_T^+)} \frac{dP_T(\delta_T^+)}{d\delta_T^+} \quad (17)$$

$$\phi_T(\delta_T^+) = - Q_T(\delta_T^+) \gamma_T - \delta_T^+ \frac{dQ_T(\delta_T^+)}{d\delta_T^+} \quad (18)$$

$$S_{iT}(y_T^+, \delta_T^+) = \frac{1}{g_{si}} \left. \frac{\partial g_{si}}{\partial \delta_T^+} \right|_{y_T^+} \quad (19)$$

$$S_{oT}(\bar{y}_T, \delta_T^+) = \frac{1}{g_{so}} \left. \frac{\partial g_{so}}{\partial \delta_T^+} \right|_{\bar{y}_T} \quad (20)$$

Observe that the variables S_{iT} and S_{oT} , as defined in Eqs. (19) and (20), represent how fast the functions g_{si} and g_{so} change with respect to δ_T^+ for a fixed y position, respectively. Both of them will vanish identically in the limit of $\delta_T^+ \rightarrow \infty$. Meanwhile, when the temperature profiles are normalized using the new scalings, as shown in Figs. 2(b) and 3(d), the temperature profiles g_{si} in inner variables and g_{so} in outer variables have a very weak dependence on δ_T^+ in the overlap region. Therefore, the following relationship $S_{oT} = S_{iT} \cong 0$ exists in the overlap region and Eq. (16) can be written as

$$\bar{y}_T \left. \frac{\partial g_{so}}{\partial \bar{y}_T} \right|_{\delta_T^+} \cong g_{so} \gamma_T + \phi_T \quad (21)$$

The solution of Eq. (21) is a first order approximation of the outer profile, g_{so} . Consequently, in the overlap region, a power law solution is obtained by integrating Eq. (21) as

$$\frac{T - T_\infty}{T_{so}} = g_{so}(\bar{y}_T, \delta_T^+) \Big|_{\text{overlap}} = C_{oT}(\delta_T^+) (\bar{y}_T + \bar{a}_T)^{\gamma_T(\delta_T^+)} + B_{oT}(\delta_T^+) \quad (22)$$

where $B_{oT}(\delta_T^+) = -\phi_T / \gamma_T$. Similarly, a power law solution expressed in inner variables can be formulated in a similar way and has the following form:

$$\frac{T_w - T}{T_{si}} = g_{si}(y_T^+, \delta_T^+) \Big|_{\text{overlap}} = C_{iT}(\delta_T^+) (y_T^+ + a_T^+)^{\gamma_T(\delta_T^+)} + B_{iT}(\delta_T^+) \quad (23)$$

where $B_{iT}(\delta_T^+) = -\varphi_T / \gamma_T$ with $\varphi_T = \delta_T^+ / P_T(dQ_T/d\delta_T^+)$, which is also a first-order approximation to the temperature profiles in the overlap region. The parameters a_T^+ and \bar{a}_T in Eqs. (22) and (23) arise from the fact that the results should be independent of the origin shift according to George and Castillo [15] and Oberlack [22]. George and Castillo [15] used a value of -16 for a^+ in the ZPG velocity profile. Here, a_T^+ and \bar{a}_T can be simply transformed from a^+ by $a_T^+ = \varepsilon a^+$ with $\varepsilon = \sqrt{\text{St}/(Cf/2)}$ and $\bar{a}_T = a^+(\delta / \delta_T^+)(1/\delta^+)$. Other coefficients such as C_{oT} , C_{iT} , γ_T , B_{iT} , and B_{oT} are the functions of δ_T^+ only. Matching the outer profile Eq. (22) and the inner profile Eq. (23) yields the following constraints given as

$$\ln \delta_T^+ \frac{d\gamma_T}{d \ln \delta_T^+} = \frac{d \ln(-C_{oT}/C_{iT})}{d \ln \delta_T^+} \quad (24)$$

and

$$B_{oT} = \delta_T^+ / \delta_T^* (1 - \text{Pr} \sqrt{\text{St}} B_{iT}) \quad (25)$$

The solutions of the constraint given in Eq. (24) are as follows:

$$\gamma_T = \gamma_{T\infty} + \frac{\alpha A}{(\ln \delta_T^+)^{1+\alpha}} \quad (26)$$

$$\frac{C_{oT}}{C_{iT}} = \frac{C_{oT\infty}}{C_{iT\infty}} \exp \left[\frac{(1+\alpha)A}{(\ln \delta_T^+)^{\alpha}} \right] \quad (27)$$

where the coefficients $A=2.9$ and $\alpha=0.46$, which use the same value as the case of the velocity profile discussed by George and Castillo [15]. The coefficients $\gamma_{T\infty}$, $C_{oT\infty}$, and $C_{iT\infty}$ are the asymptotic values of γ_T , C_{oT} , and C_{iT} . These asymptotic constants will be determined from the experimental data of Blackwell [18] in the later sections.

2.3 Temperature Profiles in the Inner Region. In the region very close to the wall, the heat conduction term is a first order term compared to convection terms in the governing equation. Monin and Yaglom [23] have shown that the Taylor expansion of the mean temperature profile in the sublayer region has the form of

$$\frac{T_w - T}{T_\tau} = \text{Pr} [y^+ - C_4(y^+)^4 + C_5(y^+)^5 + \dots] \quad (28)$$

where $T_\tau = q_w / \rho C_p \mu_\tau$. In this investigation, this Taylor's expansion will be used. A filter function of the exponential form will be adopted considering the fact that the combination of the near-wall expansion, Eq. (28), and the overlap expansion, Eq. (23), is valid up to $y^+ \cong 15$. George and Castillo [15] used a similar idea to form the inner velocity profile. An expression, which can describe the inner temperature profile, is given as

$$\begin{aligned} \frac{T_w - T}{T_w - T_\infty} = & \text{Pr St} \frac{U_\infty}{u_\tau} \underbrace{[y^+ - C_4(y^+)^4 + C_5(y^+)^5]}_{\text{near-the-wall region}} \exp[-d(y^+)^6] \\ & + \text{Pr} \sqrt{\text{St}} (1 - \exp[-d(y^+)^6]) \\ & \times \underbrace{\left\{ C_{iT} y_T^{+\gamma_T} \left[1 + \gamma_T a_T^+ y_T^{+1} + \frac{1}{2} \gamma_T (\gamma_T - 1) a_T^{+2} y_T^{+2} \right] + B_{iT} \right\}}_{\text{overlap region}} \end{aligned} \quad (29)$$

in which the coefficients $C_4 \cong 1 \times 10^{-4}$, $C_5 \cong 3 \times 10^{-6}$, and the damping coefficient $d = 1 \times 10^{-7}$ were obtained from the experimental data in the inner region ($0 \leq y^+ \leq 15$).

2.4 Temperature Profiles in the Outer Region. In order to ensure that the temperature profile is best represented in the wake region and that all the boundary conditions are satisfied, a polynomial wake function is proposed. In the present investigation, the suggested thermal wake function takes the polynomial form of $w_T(\bar{y}_T) = w_m \bar{y}_T^2 + w_n \bar{y}_T^3$, which is similar to the one used by Kader [5] and Granville [24]. Combining the power law solution in the overlap region in outer variables and the new wake function, the outer composite temperature profile is then given as,

$$\frac{T - T_\infty}{T_w - T_\infty} = \underbrace{\frac{\delta_T^*}{\delta_T} [C_{oT}(\bar{y}_T + \bar{a}_T)^{\gamma_T} + B_{oT}]}_{\text{overlap region}} + \underbrace{\frac{w_T(\bar{y}_T)}{w_T(\bar{y}_T)}}_{\text{wake region}} \quad (30)$$

The coefficients w_m and w_n appearing in the wake function $w(\bar{y}_T)$ depend on δ_T^+ , which is contrary to the assumed constant values given as $w_m = 6$ and $w_n = -4$, by Kader [5] and Granville [24]. In the present derivation, the coefficients w_m and w_n are determined such that they satisfy the boundary layer conditions given as

$$y = \delta_T \text{ (or } \bar{y}_T = 1) \Rightarrow \frac{dT}{dy} = 0 \quad \frac{T - T_\infty}{T_w - T_\infty} = 0 \quad (31)$$

Thus, using the above boundary conditions, Eqs. (31) and (30), the analytical forms of w_m and w_n are obtained as

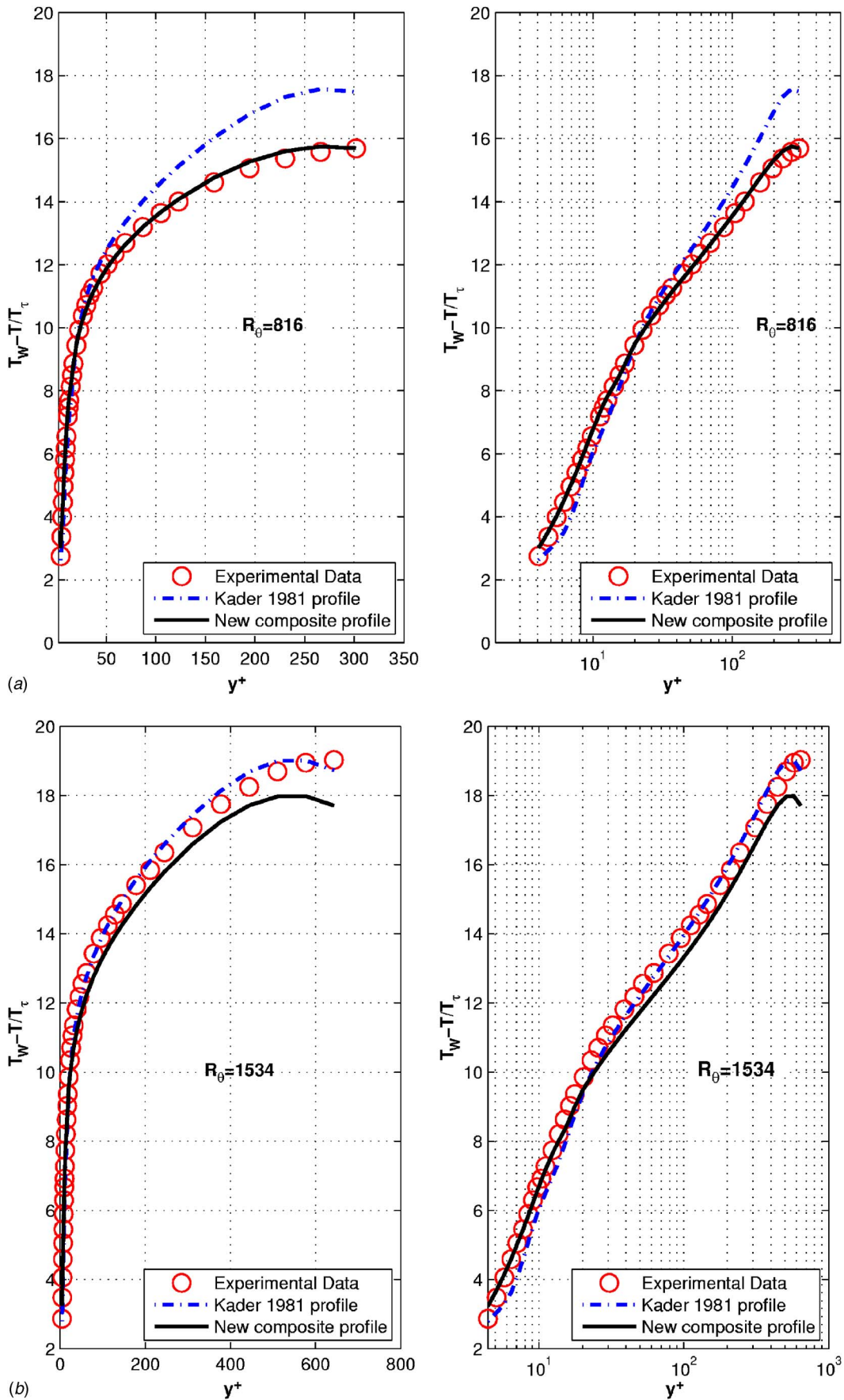


Fig. 4 The composite temperature profile of ZPG flows: Blackwell [18]

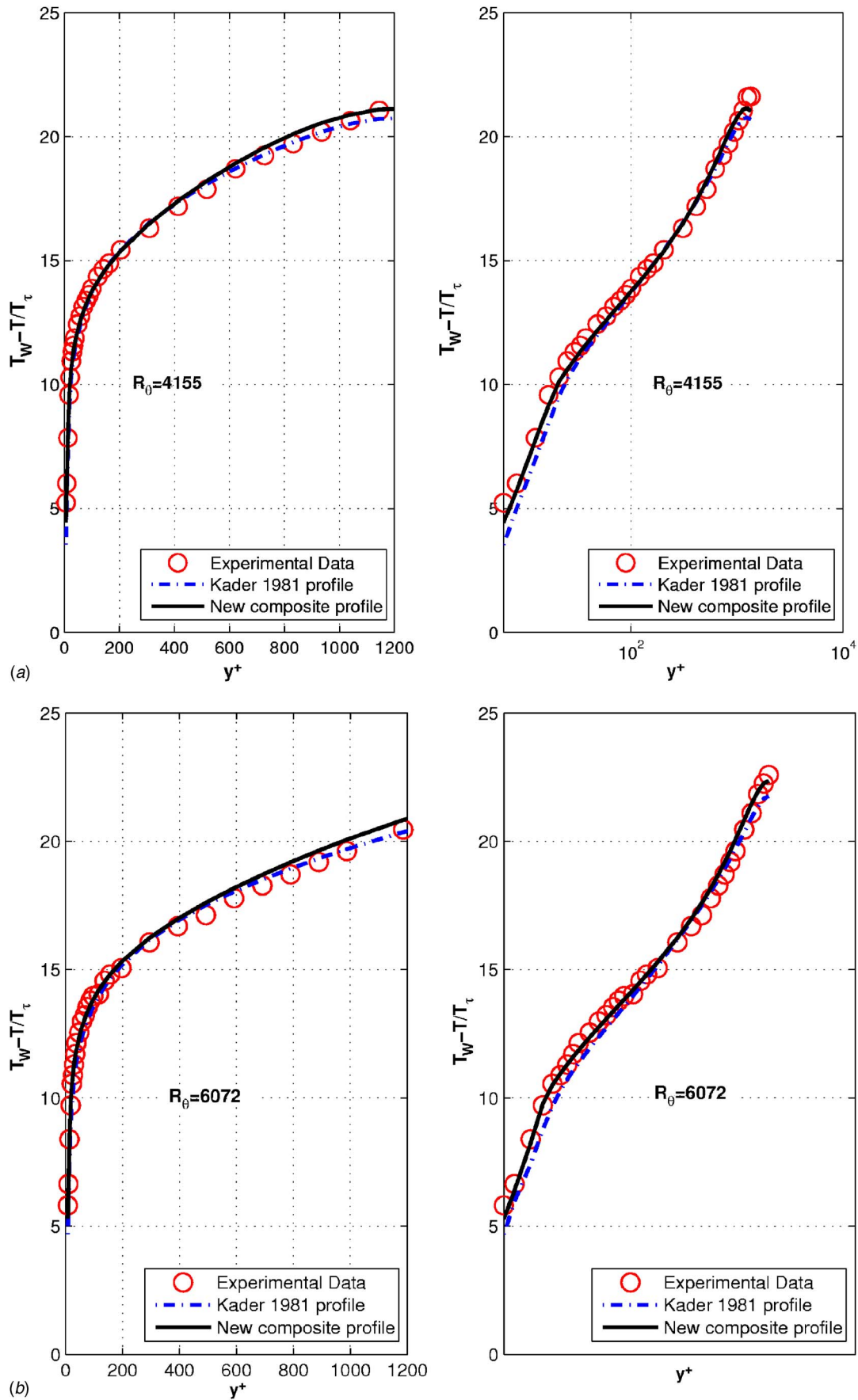


Fig. 5 The composite temperature profile of ZPG flows: Reynolds [19]

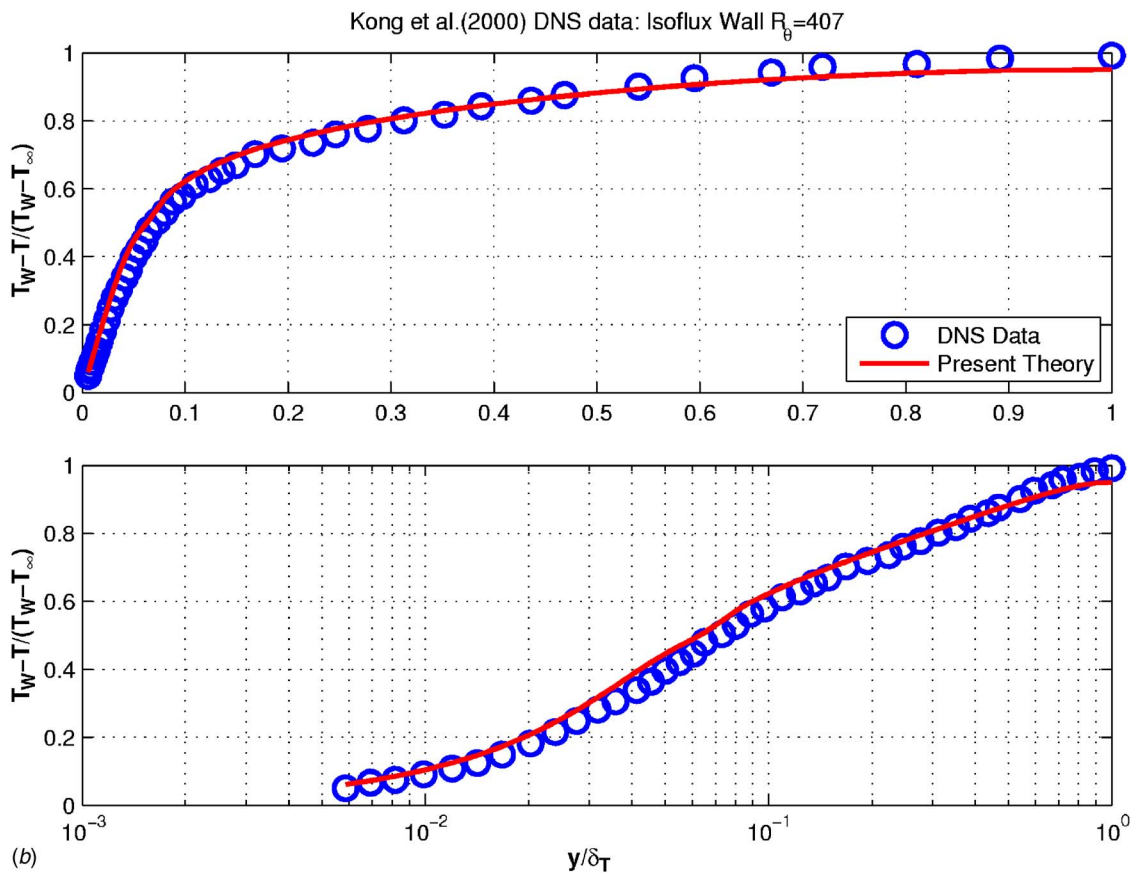
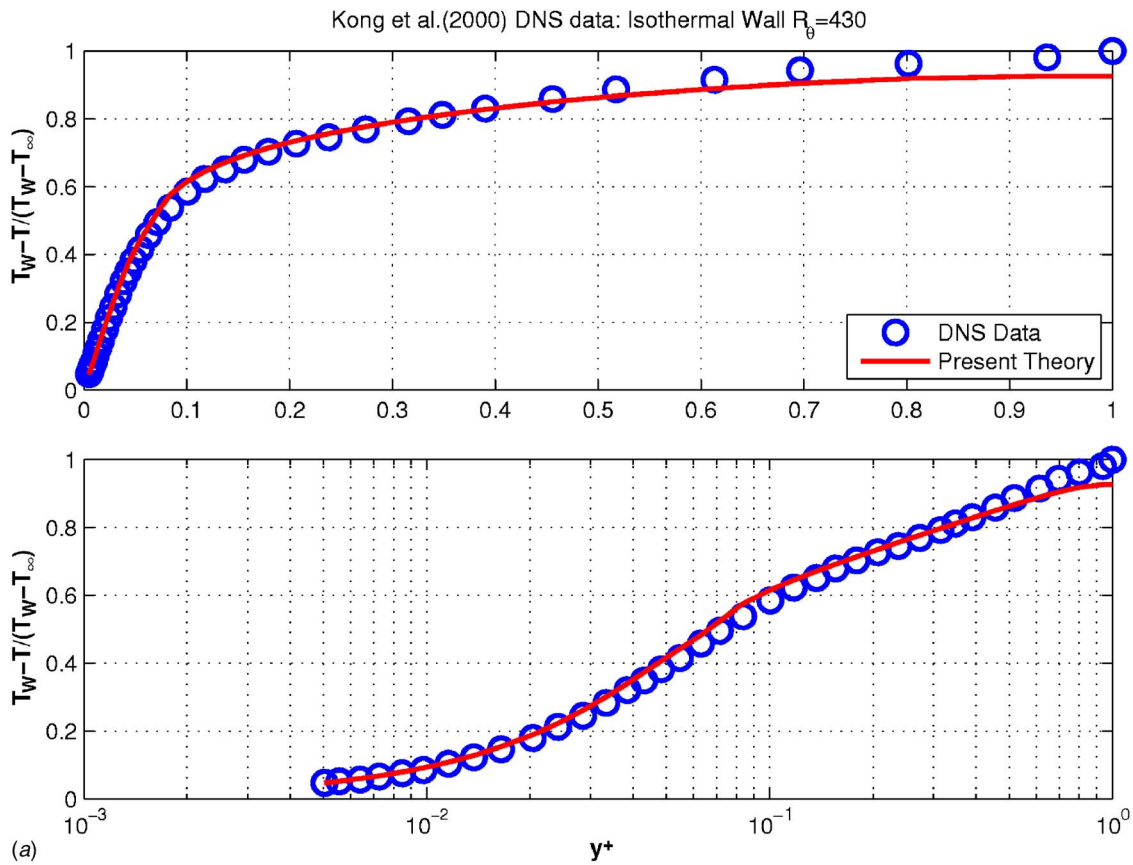


Fig. 6 The composite temperature profile of DNS data for ZPG flows: Kong et al. [20]

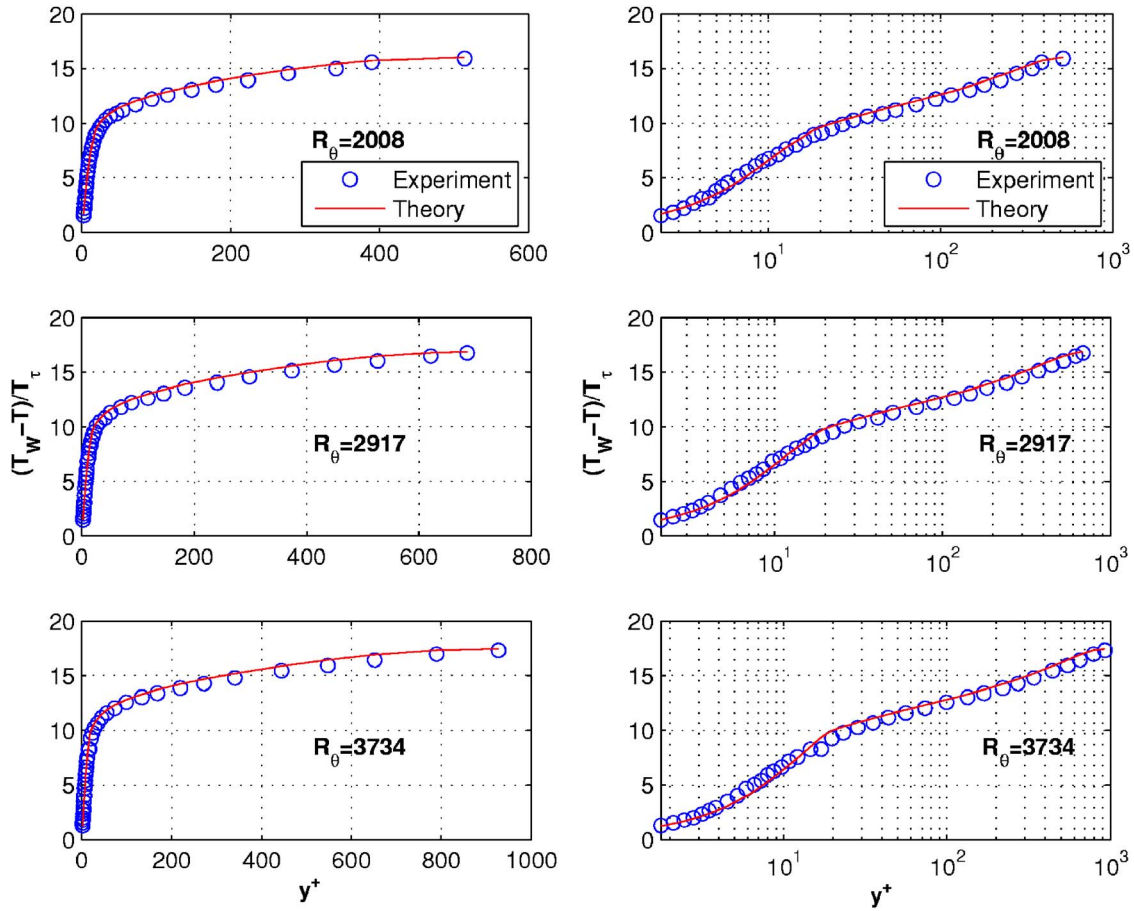


Fig. 7 The new composite temperature profile for APG flow: Blackwell [18] $m = -0.15$

$$w_m = -\frac{\delta_T^*}{\delta_T} [3C_{oT}(1 + \bar{a}_T)^{\gamma_T} + 3B_{oT} - C_{oT}\gamma_T(1 + \bar{a}_T)^{\gamma_T-1}] \quad (32)$$

$$w_n = -\frac{\delta_T^*}{\delta_T} [C_{oT}\gamma_T(1 + \bar{a}_T)^{\gamma_T-1} - 2C_{oT}(1 + \bar{a}_T)^{\gamma_T} - 2B_{oT}] \quad (33)$$

where δ_T^*/δ_T is actually an integration of the dimensionalized temperature profile from the inner wall to the boundary layer edge. A constant value of $\delta_T^*/\delta_T \approx 1.45$ is obtained from the experimental data of Blackwell [18]. This constant value will be used for the other data as well.

2.5 Composite Temperature Profiles. Using the inner temperature profile, Eq. (29), and the outer temperature profile, Eq. (30), it is possible to construct a composite profile that describes the entire boundary layer at the finite δ_T^* number. This composite temperature profile is composed of the inner profile and the outer profile, but the profile in the overlap region, Eq. (22) or (23), has to be subtracted once to avoid repeating according to Van Dyke [25]. Hence, the composite temperature profile can be constructed in terms of the outer variables as

$$\frac{T_W - T}{T_W - T_\infty} = \underbrace{\left[1 - \frac{\delta_T^*}{\delta_T} g_{so}(\bar{y}_T, \delta_T^*) \right]}_{\text{outer region}} + \Pr \sqrt{\text{St}} \underbrace{\left[g_{si}(\bar{y}_T \hat{\delta}_T^+, \delta_T^*) \right]}_{\text{inner region}} - \underbrace{C_{iT}(\bar{y}_T \hat{\delta}_T^+ + a_T^+)^{\gamma_T} - B_{iT}}_{\text{overlap region}} \quad (34)$$

Notice that the inner length scale y^+ can be expressed in outer variables as $y^+ = (\delta_T U_\tau / \nu) \bar{y}_T = \bar{y}_T \hat{\delta}_T^+$. Thus, using Eqs. (29)–(33),

the composite profile, Eq. (34), can be rewritten in inner variables as

$$\begin{aligned} \frac{T_W - T}{T_\tau} = \frac{T_W - T_\infty}{T_\tau} & \left\{ -[w_m(y^+/\hat{\delta}_T^*)^2 + w_n(y^+/\hat{\delta}_T^*)^3] + \Pr \text{St} \frac{U_\infty}{U_\tau} \right. \\ & \times \exp[-dy^{+6}] [y^+ - C_4 y^{+4} + C_5 y^{+5}] \\ & + \Pr \sqrt{\text{St}} \left\{ B_{iT} + C_{iT}(y^+\varepsilon)^{\gamma_T} \left[1 + \gamma_T a_T^+(y^+\varepsilon)^{-1} \right. \right. \\ & \left. \left. + \frac{1}{2} \gamma_T (\gamma_T - 1) a_T^{+2} (y^+\varepsilon)^{-2} \right] \right\} \left. \left\{ 1 - \exp[-dy^{+6}] \right\} \right\} \quad (35) \end{aligned}$$

In order to use Eq. (35), the variables listed in Table 1 should be obtained from the experiments or prescribed.

This profile will be verified with the experimental data and the DNS data, and will be compared with the theoretical profile of Kader [5] shown in the Appendix of this paper.

3 Results

3.1 Coefficients of the Composite Temperature Profiles. In order to describe the experimental data using the composite pro-

Table 1 Variables collected from experimental data

Temperature information	T_W, T_τ, T_∞
Velocity information	U_τ, U_∞
Property of fluids	\Pr, ν, ρ
Boundary layer information	δ, δ_T^*

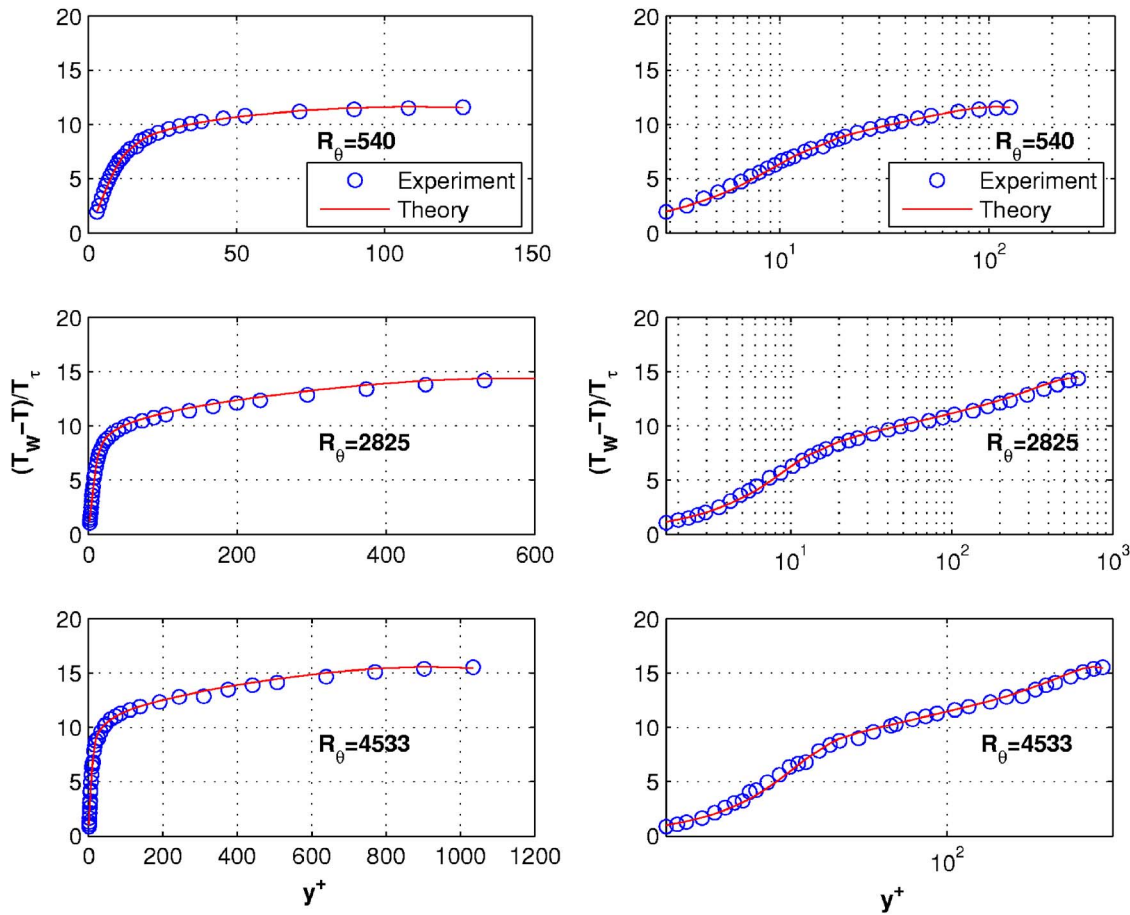


Fig. 8 The new composite temperature profile for APG flow: Blackwell [18] $m=-0.2$

file, Eq. (35), the correlations of C_{oT} , C_{iT} , and γ_T need to be determined along with the constraints enforced by Eq. (24). By optimizing the experimental data of Blackwell [18], it was found that the outer coefficients B_{oT} and C_{oT} can be approximately described as

$$\frac{C_{oT}}{C_{oT\infty}} = 1 - 1.32 \exp(-0.0226 \delta_T^+) \quad (36)$$

$$\frac{B_{oT}}{B_{oT\infty}} = 1 - 0.4 \exp(-0.0049 \delta_T^+) \quad (37)$$

where $B_{oT\infty}=5.05$ and $C_{oT\infty}=-4.67$ for APG boundary layer flow and $B_{oT\infty}=5.9$ and $C_{oT\infty}=-5.4$ for ZPG boundary layer flow. Then, using Eqs. (27) and (36), $C_{iT}/C_{iT\infty}$ is now given as

$$\frac{C_{iT}}{C_{iT\infty}} = [1 - 1.32 \exp(-0.0226 \delta_T^+)] \exp\left[\frac{(1 + \alpha)A}{(\ln \delta_T^+)^{\alpha}}\right] \quad (38)$$

Using the constraint given by Eqs. (25) and (37), B_{iT} is then given as

$$B_{iT} = \frac{1}{\text{Pr} \sqrt{\text{St}}} \left\{ 1 - \frac{\delta_T^*}{\delta_T} B_{oT\infty} [1 - 0.4 \exp(-0.0049 \delta_T^+)] \right\} \quad (39)$$

Note that the slight difference of the coefficients between the APG and ZPG flows is due to major effects of the pressure gradient on the outer flow. The asymptotic value of the power coefficient $\gamma_{T\infty}$ is found to be a constant of 0.0827, which is same for both ZPG and APG flows considered here. Table 2 summarizes the coefficients for the composite profile, Eq. (35), for all the experimental data by Blackwell [18] with both ZPG and APG.

3.2 Temperature Profiles. Figure 4 compares Kader's composite profile given in the appendix with the new composite profile of Eq. (35) for the ZPG experimental data of Blackwell [18]. The reason why we used the composite profile in the inner variable is that it is convenient to compare the new results with Kader's results since the composite profile proposed by Kader is given in inner variables. In Fig. 4, the circle represents the experimental data, the dash line Kader's log-law composite profile, and the solid line the current power law composite profile. Notice that the new composite profile can describe the experimental data through the entire boundary layer within an error of less than 5%, while Kader's log law with an average error of 8%. Especially, Kader's log-law composite profile cannot predict the low Reynolds number flow well in the outer region as magnified in Fig. 4.

Figure 5 shows the ZPG experimental data of Reynolds [19] for the new composite profile of Eq. (35) and Kader's composite profile (details of this function can be found in the Appendix). Reynolds's experiment focused exclusively on the convective heat

Table 2 The values of various coefficients in the composite profile

C_4	C_5	d	α	A
1×10^{-4}	3×10^{-6}	1×10^{-7}	0.46	2.9
$\gamma_{T\infty}$	$\frac{C_{oT\infty}}{C_{iT\infty}}$	$B_{oT\infty}$	$C_{oT\infty}$	
0.0829	-0.12	5.9(ZPG) 5.05(APG)	-5.4 (ZPG) -4.67 (APG)	

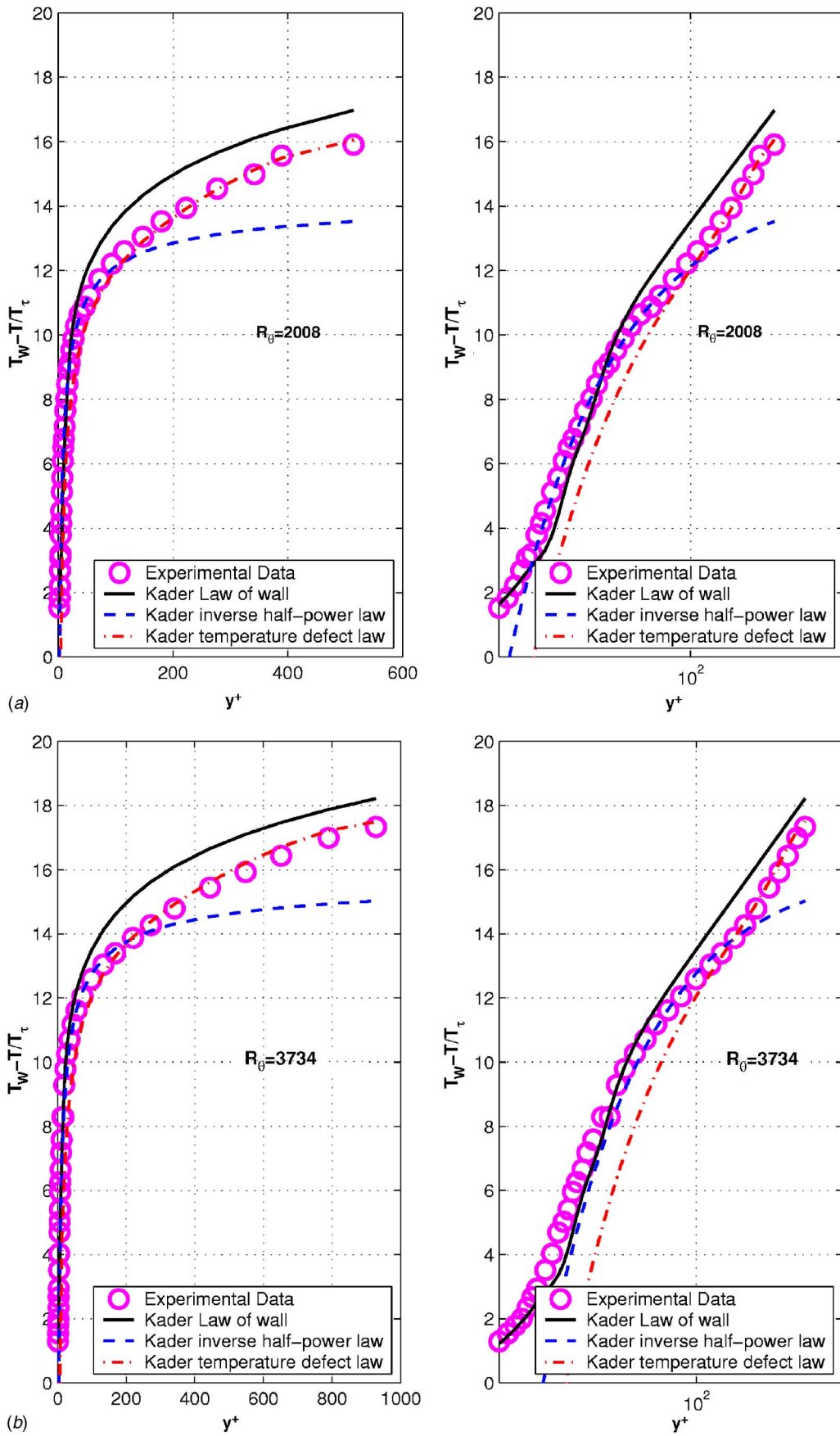


Fig. 9 Kader's composite temperature profile for APG flows: Blackwell [18] $m = -0.15$

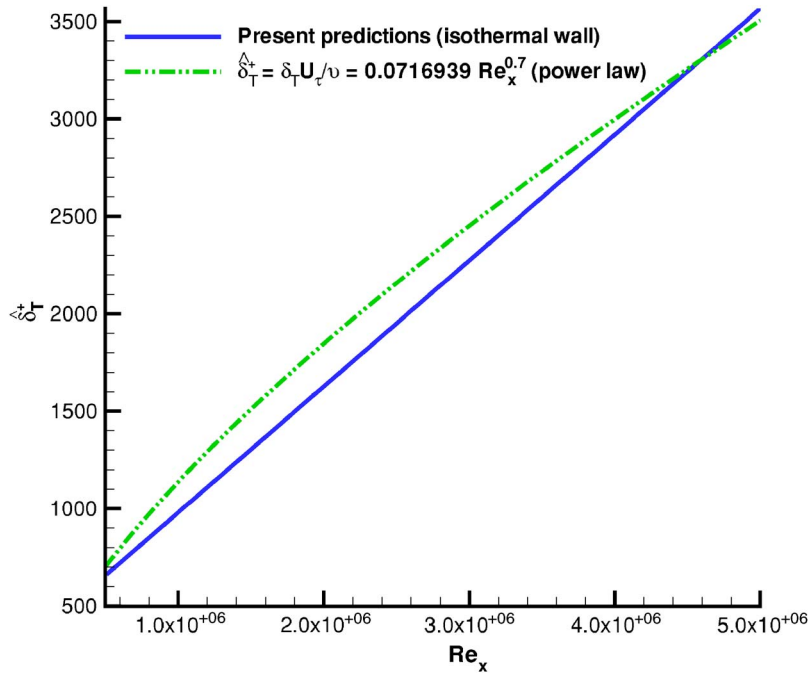


Fig. 10 Reynolds number based on the thermal boundary layer thickness versus Reynolds number based on the x coordinate

transfer from a flat plate (i.e., there is no change in the external pressure). The upstream velocity is around 30 m/s and the Reynolds number based on the momentum thickness is up to 6072. As shown in Fig. 5, the new composite profile performs better than Kader's profile in describing the experimental data, especially in the inner region. It is important to observe that this set of data was not used at all in calculating the coefficients shown in Table 2. Therefore, the accuracy of the composite profile (at least for the ZPG flow) is actually independent of the data used (i.e., Blackwell data). Moreover, it can also be generalized to describe the data with different Reynolds numbers.

Furthermore, Fig. 6 shows another independent verification of the proposed temperature profile using the DNS data by Kong et al. [20] for $Re_\theta=407$ and $Re_\theta=430$. Figure 6(a) shows the comparisons of the ZPG flow data on an isothermal condition and the proposed composite profile. The new composite profile can predict this DNS temperature profile very well with an average error of less than 2%. Particularly, the proposed composite profile can predict the inner region and overlap region very well. In the wake region, the maximum error between the theory and the DNS data is 8.3%. Similarly, Fig. 6(b) shows the comparison between the proposed temperature profile and the DNS data with a constant heat flux condition. The average error between these two profiles is less than 5%. However, in the near-wall region, the maximum error between the theory and the DNS data is up to 18%, which is mainly due to the fact that at such low Reynolds number, the boundary layer does not have an overlap region and is mainly composed of mesolayer.

Figures 7 and 8 show the results using the new composite profile Eq. (35) for APG flows subject to different strengths of the pressure gradients with $m=-0.15$ and $m=-0.2$, respectively. As shown in these figures, a single new composite profile can describe the entire boundary layer very well, and the average error is less than 5%. Also, a single value of each coefficient listed in Table 2 works for both APG and ZPG flows but with different Reynolds numbers.

Figure 9 shows some examples of the same experimental data but using Kader's temperature profiles [5]. The circle represents the experimental data, the solid line Kader's law of the wall (i.e.,

Eq. (1) in the Appendix), the dash line Kader's inverse half-power law (i.e., Eq. (A2) in the Appendix), and the dash dot line Kader's defect law (i.e., Eq. (A3) in Appendix). Notice that the exact region where each of these laws is valid cannot be determined beforehand. Therefore, each of these profiles is plotted here through the entire boundary layer. As shown in the semilog plot on the right side, Kader's defect law can only describe the outer part of the boundary layer. Kader's inverse half-power law shows a good fit for the data in the "overlap" region. However, Kader's log law shows a poor prediction in the near-wall region, which is very important in predictions of heat transfer on the wall. Therefore, the new composite profile has the obvious advantages over Kader's profiles in describing the entire boundary layer profile, especially the inner region, which is very crucial to predict the heat transfer law.

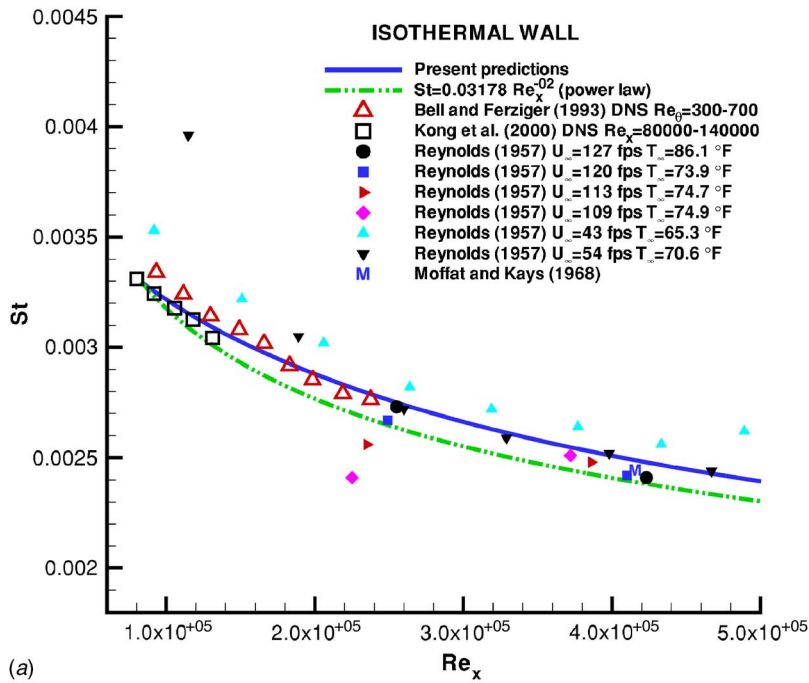
3.3 Heat Transfer Law. The current composite temperature profile can be applied to derive the heat transfer law. Using the integral forms of the momentum and energy equations, the Stanton number is solved for turbulent boundary layers over a flat surface.

The integral forms of momentum and energy equations in inner variables are given below as

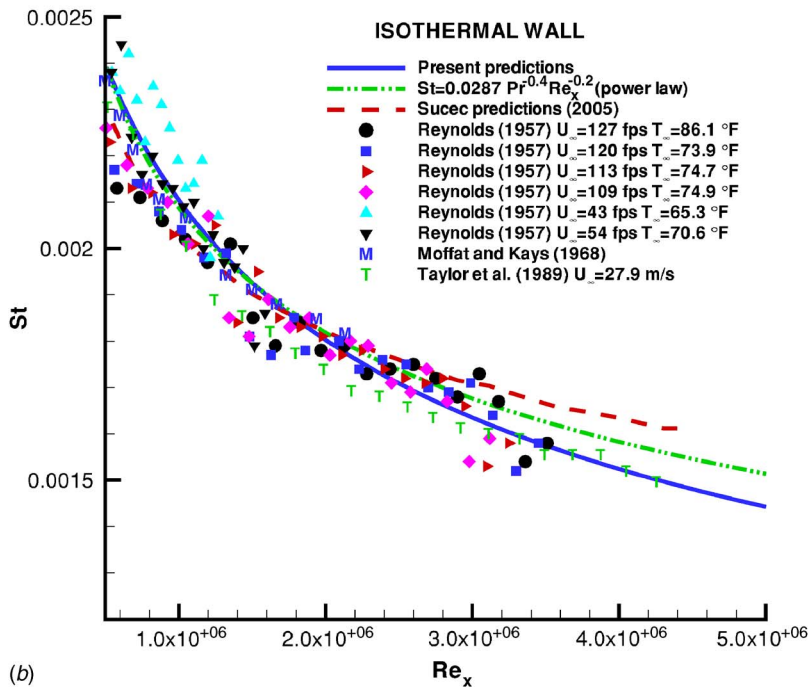
$$\frac{d}{dRe_x} \left[\frac{1}{(u_\tau U_\infty)} \int_0^{\delta^+} \frac{U}{U_\infty} \left(1 - \frac{U}{U_\infty} \right) dy^+ \right] = \left(\frac{u_\tau}{U_\infty} \right)^2 \quad (40)$$

$$\frac{d}{dRe_x} \left[\frac{q_w}{(u_\tau U_\infty)^2} \int_0^{\delta^+} \frac{U}{U_\infty} \left[\left(\frac{T_w - T_\infty}{T_\tau} \right) - \left(\frac{T_w - T}{T_\tau} \right) \right] dy^+ \right] = q_w \quad (41)$$

First, the momentum equation (40) is solved by considering a Runge-Kutta procedure and using the velocity composite profile, UU_∞ , as well as an expression for $u_\tau U_\infty$ as a function of δ^+ , developed by George and Castillo [15]. In this way, the variation of the hydrodynamic boundary layer thickness as a function of the



(a)



(b)

Fig. 11 Stanton number calculated by the composite temperature profile and the integral energy equation for the isothermal data

streamwise direction x (or $Re_x = xU_\infty/\nu$) is calculated along the flat plate.

Then, with the hydrodynamic solution ($\delta = f(Re_x)$), the corresponding velocity profile by George and Castillo [15] and the temperature profiles developed in the present analysis given by Eq. (35), the energy equation (41) is solved in a similar manner to determine the variation of the thermal boundary layer thickness along the flat plate. Figure 10 shows the variation of the thermal boundary layer thickness normalized by the friction velocity versus the Reynolds number based on the x coordinate ($Re_x = xU_\infty/\nu$) for a boundary layer flow on a flat with an isothermal wall. A comparison is performed with an empirical equation obtained

from different power law curves proposed by White [26]. By using equations from White's [26] (i.e., Eqs. (6-112a) and (6-112b) of book) plus a hydrodynamic/thermal boundary layer thickness ratio in a flat plate at $Pr=0.7$, the following expressions are obtained:

$$C_f = 0.0592 Re_x^{-1/5} \quad (42)$$

$$\frac{\delta}{x} = 0.37 Re_x^{-1/5} \quad (43)$$

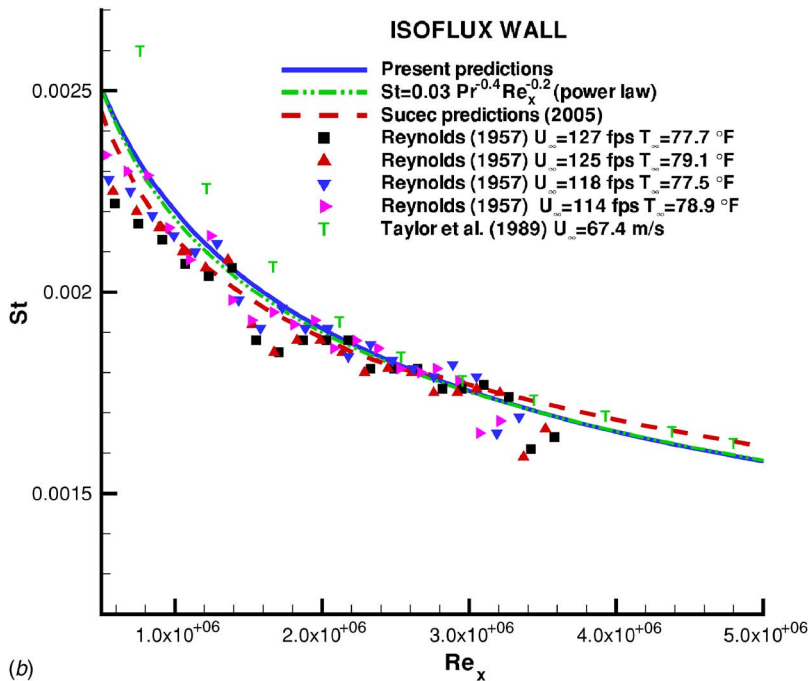
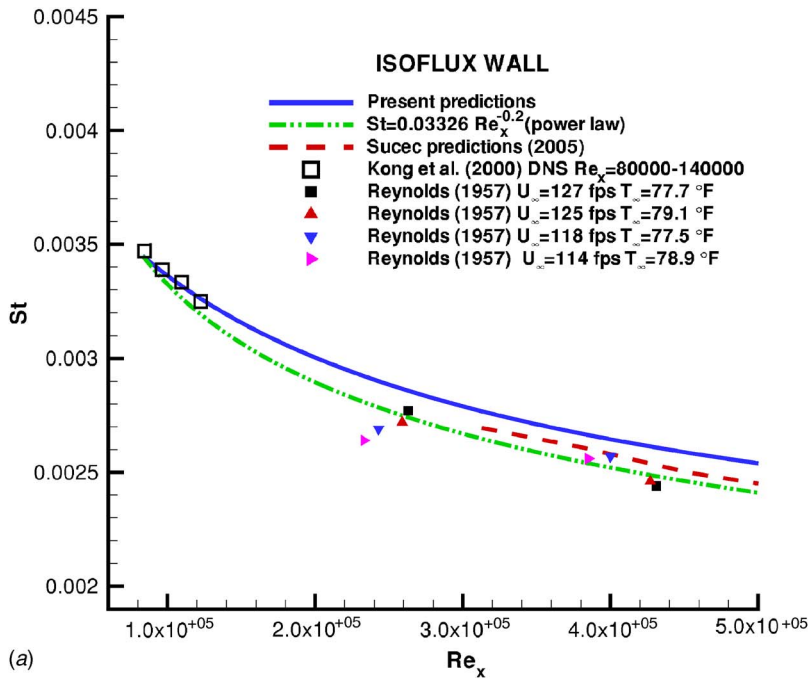


Fig. 12 Stanton number calculated by the composite temperature profile and the integral energy equation for the isoflux data

$$\frac{\delta}{\delta_T} \approx Pr^{1/3} \quad (44)$$

$$\hat{\delta}_T^+ = 0.0716939 Re_x^{0.7} \quad (45)$$

According to Fig. 10, the maximum relative error is approximately 15% at Re_x equal to 2×10^6 . For the range of Reynolds numbers considered, i.e., from 5×10^5 to 5×10^6 , the average uncertainty is approximately 5%.

In solving both governing equations, it is necessary to start the marching process along the flat plate from a known point or initial conditions, i.e., finite values of the velocity and thermal boundary layer thicknesses must be specified at some location. At the lead-

ing edge of the flat plate, both thicknesses are considered zero. To avoid the discontinuity of the Stanton number at this point (infinity), calculations are started from a downstream point.

Finally, the thermal solution $\delta_T^+ = f(Re_x)$ is substituted into the heat transfer law given as below

$$\sqrt{St} = \frac{1}{Pr} \frac{\partial_T^*}{\partial_T} \left(-\frac{C_{oT\infty}}{C_{iT\infty}} \right) \exp \left[\frac{A}{(\ln \delta_T^+)^{\alpha}} \right] \delta_T^{+ - \gamma T_{\infty}} \quad (46)$$

which is obtained by matching the outer profile, Eq. (22), and the inner profile, Eq. (23), in the overlap region.

The roots of the nonlinear equation (46) are solved by the bi-section method and represent the Stanton numbers at different Reynolds numbers.

Figures 11 and 12 show a comparison of the Stanton number predictions on air as a function of the Reynolds number based on the x coordinate with an empirical power law, numerical results, and experimental data. All data are grouped according to different wall conditions (isothermal and isoflux) and Reynolds numbers (low and high).

Figure 11(a) shows the results of Stanton numbers obtained at low Reynolds numbers ($80,000 < Re_x < 500,000$) for an isothermal wall. A comparison is made with the empirical power law for low Re_x from Kays and Crawford [27], the DNS results from Bell and Ferziger [28] and Kong et al. [20], and experimental data from Reynolds [19] and Moffat and Kays [29]. The maximum deviation of the present predictions from the power law is around 4.3% at $Re_x \sim 250,000$. However, the present predictions depict a better agreement with DNS results as well as with experimental data than the power law. Similarly, for the isoflux wall condition at low Re_x , as shown in Fig. 11(b), it is observed that there is a good agreement with DNS data from Kong et al. [20]. On the other hand, as the Re_x increases, the power law is a little bit closer to the experimental data from Reynolds [19] and Sucec's predictions [30] (who used the combined law of the wall and the wake function of Coles for solving the integral forms of the momentum and energy equations) than our predictions.

Figure 12(a) depicts the results for the isothermal boundary condition at high Re_x . The present predictions show a good agreement with the power law curve from Kays and Crawford [27] (i.e., Eqs. (12)–(14) of the book, which are valid for the range $500,000 < Re_x < 5,000,000$). At higher Reynolds numbers, a slight increasing separation of the present calculations with respect to the empirical profile is observed; however, a similar trend is seen in Sucec's predictions [30]. However, the present simulations show a better agreement in this zone of high Reynolds numbers with experimental data from Taylor et al. [31] than those of Sucec [30]. Experimental data from Reynolds [19] exhibit a significant level of dispersion, which is probably due to the different upstream conditions considered. In a similar way, Figure 12(b) shows the variation of the Stanton number at high Re_x but at an isoflux wall condition. An almost perfect agreement between the present predictions and the empirical power law from Kays and Crawford [27] (i.e., Eqs. (12)–(27), which are valid for the range $500,000 < Re_x < 5,000,000$) is appreciated. When comparing with experimental data from Taylor et al. [31], some disagreement is obtained at lower Reynolds numbers (in the range $500,000 < Re_x < 1,500,000$). A better match with experimental data from Taylor et al. [31] is observed at higher Reynolds numbers, not only for our numerical predictions but also for the Sucec's calculations. As in the isothermal case, Reynolds' experiments [19] show some dispersion, which can be reached a maximum deviation of 6% with respect to the power law. Therefore, an accurate comparison becomes difficult. In general, present predictions and Reynolds' experiments [19] show a similar trend, especially in the range of $Re_x = 1,800,000 - 3,000,000$.

4 Conclusions

Two temperature scalings, proposed by Wang and Castillo [17], were reviewed and applied for the forced convection turbulent boundary layer by using the theory of similarity analysis and the analogy between the momentum and energy transport equations. The new temperature scalings were shown to be able to collapse the temperature profile better than the single temperature scaling proposed in the classical theory. Particularly, these scalings were able to remove the effects of Reynolds number dependence and pressure gradient on both inner and outer flows. Using the near-asymptotic theory and the new temperature scalings, a new power law solution has been obtained for the temperature profile in the overlap region by matching the inner and outer temperature pro-

files. Moreover, a function describing the inner region was proposed similar to the inner velocity profile proposed by George and Castillo [15], and a new wake function was proposed, which satisfies the boundary conditions in the outer region of the boundary layer. Furthermore, a composite temperature profile was formed, which is able to describe the flow over the entire boundary layer at finite Reynolds number.

This new composite temperature profile was verified by using the experimental data, the DNS data, and the theoretical profile by Kader [4,5]. It was shown that the present temperature profile shows a better prediction with an average error of less than 5% than Kader's prediction for the the same experimental data. The new composite temperature profile was also independently verified using the DNS data and the experimental data from Reynolds [19], which were not used in determining the coefficients in the temperature profile. As a result, the new composite profile shows a very good agreement with experimental and DNS data with an average error of less than 5%.

Furthermore, the new temperature composite profile was combined with the integral momentum and energy equation to calculate the Stanton number and the boundary layer growth along the streamwise direction. Various DNS data and experimental data under isothermal or isoflux boundary conditions have been used to test the newly calculated Stanton number, respectively. It was shown that the Stanton number in the power law form can predict the experimental data or the DNS data with an average error of 5%.

Acknowledgment

The authors are very thankful to Dr. Ramona Travis from NASA Stennis Space Center for her continuous support of many of our projects.

Nomenclature

$C_f/2$	= skin friction coefficient
g_{so}, g_{si}	= outer and inner temperature functions
Pr	= Prandtl number, $Pr = \nu / \alpha$
Pe	= Peclet number, $Pe = U_\infty \delta / \alpha$
Re_δ	= Reynolds number, $Re_\delta = U_\infty \delta / \nu$
Re_θ	= Reynolds number based on momentum thickness, $Re = U_\infty \theta / \nu$
Re_x	= Reynolds number based on streamwise direction x , $U_\infty x / \nu$
Re_{δ_T}	= Reynolds number based on thermal boundary layer thickness δ_T , $U_\infty \delta_T / \nu$
St	= Stanton number, $St = q_w / \rho C_p U_\infty (T_w - T_\infty)$
T_{so}, T_{si}	= outer and inner temperature scaling
T_τ	= friction temperature, $T_\tau = q_w / \rho C_p u_\tau$
T_∞	= free stream temperature
T_w	= wall temperature
U_∞	= free stream velocity
u_τ	= friction velocity, $u_\tau = \sqrt{\tau_w / \rho}$
\bar{y}	= outer velocity similarity length scale, y / δ
\bar{y}_T	= outer temperature similarity length scale, y / δ_T
y^+	= inner velocity similarity length scale, $y U_\tau / \nu$
y_T^+	= inner temperature similarity length scale, $y U_\infty / \nu \sqrt{St}$

Greek Symbols

α	= thermal diffusivity, $\alpha = k / \rho C_p$
δ	= momentum boundary layer thickness, i.e., δ_{99}
δ_τ^*	= thermal boundary layer thickness
δ_T^*	= thermal displacement thickness, $\delta_T^* = \int_0^\infty T - T_\infty / T_w - T_\infty dy$
δ_T^+	= ratio of outer to inner temperature length scales, i.e., $\delta_T U_\infty / \nu \sqrt{St}$

δ_T^+ = ratio of classical outer to inner temperature length scales, i.e., $\delta_T U_\tau / \nu$
 ν = kinematic viscosity, μ / ρ

Subscripts

si = inner thermal boundary layer
 so = outer thermal boundary layer
 W = at the wall
 ∞ = free stream

Appendix

Kader [5] proposed the temperature profile for the turbulent boundary layer with pressure gradient. He divided the pressure gradient flow in three regions, and each region is characterized by the following equations:

- the inner region: $0 \leq y^+ \leq y_1 u_*^+ / \nu$ (the thermal law of the wall),

$$\frac{T_w - T}{T_\tau} = \text{Pr } y^+ \times \exp(-G) + \{\beta(\text{Pr}) + 2.12 \ln(1 + y^+)\} \exp(-1/G) \quad (\text{A1})$$

- the pressure gradient region: $y_1 \gamma / u_*^2 \leq \xi \leq y_2 \gamma / u_*^2$ (the inverse-half-power law)

$$\frac{T_w - T}{T_\tau} = -K_1^{(\theta)} / \sqrt{\xi} + K_2^{(\theta)} \quad (\text{A2})$$

- the outer region: $y_2 / H \leq \eta \leq 1$ (the temperature defect law)

$$\frac{T_w - T}{T_\tau} = \frac{T_w - T_o}{T_\tau} - \frac{3\sqrt{Z}}{1 + Z} \left(\frac{1}{\eta} - 1 \right) + \frac{2.12}{1 + Z} \ln \eta - \frac{15 - 3.5\sqrt{Z}}{20 + Z} (2 - 6\eta^2 + 4\eta^3) \quad (\text{A3})$$

where the coefficients G , $\beta(\text{Pr})$, $K_1^{(\theta)}$, $K_2^{(\theta)}$, the length scales ξ , η , Z , and the pressure parameter $\gamma = 1/\rho |dP/dx|$ can be found in Kader [5]. The vertical position y_1 is the ordinate of the intersection point for the law of the wall, Eq. (A1), and the inverse half-power law, Eq. (A2). The position y_2 represents the intersection point of the inverse half-power law and the temperature defect law, Eq. (A3). However, y_1 and y_2 cannot be determined unless the experimental data are plotted for all three regions. This is a major disadvantage of Kader's profile since these points (y_1 or y_2) may depend on the Pe number. It is worthwhile mentioning that Kader's work includes the effects of different Pr numbers.

References

[1] Gad-el-Hak, M., 2000, *Flow Control: Passive, Active and Reactive Flow Management*, Cambridge University Press, Cambridge.
 [2] Perry, A. E., Bell, J. B., and Joubert, P. N., 1966, "Velocity and Temperature Profiles in Adverse Pressure Gradient Turbulent Boundary Layers," *J. Fluid Mech.*, **25**, pp. 299–320.
 [3] Afzal, N., 1982, "Thermal Turbulent Boundary Layer Under Strong Adverse

Pressure Gradient Near Separation," *J. Heat Transfer*, ASME J. Heat Transfer **104**, pp. 397–402.

[4] Kader, B. A., 1981, "Temperature and Concentration Profiles in Fully Turbulent Boundary Layers," *Int. J. Heat Mass Transfer*, **24**, pp. 1541–1544.
 [5] Kader, B. A., 1991, "Heat and Mass Transfer in Pressure-Gradient Boundary Layers," *Int. J. Heat Mass Transfer*, **34**, pp. 2837–2857.
 [6] Erm, L. P., and Joubert, P. N., 1991, "Low-Reynolds-Number Turbulent Boundary Layers," *J. Fluid Mech.*, **230**, pp. 1–44.
 [7] Castillo, L., and Johansson, G., 2002, "The Effects of the Upstream Conditions in a Low Reynolds Number Turbulent Boundary Layer With Zero Pressure Gradient," *J. Turbul.*, **3**, pp. 1–19.
 [8] Castillo, L., and Walker, D., 2002, "The Effect of the Upstream Conditions on the Outer Flow of Turbulent Boundary Layers," *AIAA J.*, **40**, pp. 1292–1299.
 [9] Churchill, S. W., and Chan, C., 1995, "Turbulent Flow in Channels in Terms of the Turbulent Shear and Normal Stresses," *AIChE J.*, **41**, pp. 2513–2521.
 [10] Churchill, S. W., Yu, B., and Kawaguchi, Y., 2005, "The Accuracy and Parametric Sensitivity of Algebraic Models for Turbulent Flow and Convection," *Int. J. Heat Mass Transfer*, **48**, pp. 5488–5503.
 [11] Le, P. M., and Papavassiliou, D. V., 2006, "On Temperature Prediction at Low Re Turbulent Flows Using the Churchill Turbulent Heat Flux Correlation," *Int. J. Heat Mass Transfer*, **49**, pp. 3681–3690.
 [12] Wei, T., Fife, P., Klewicki, J., and McMurtry, P., 2005, "Properties of the Mean Momentum Balance in Turbulent Boundary Layer, Pipe and Channel Flows," *J. Fluid Mech.*, **522**, pp. 303–327.
 [13] Wei, T., Fife, P., Klewicki, J., McMurtry, P., 2005, "Scaling Heat Transfer in Fully Developed Turbulent Channel Flow," *Int. J. Heat Mass Transfer*, **48**, pp. 5284–5296.
 [14] George, W. K., 1995, *Some New Ideas for Similarity of Turbulent Shear Flows, Turbulence, Heat and Mass Transfer*, Begell House, New York.
 [15] George, W. K., and Castillo, L., 1997, "Zero Pressure Gradient Turbulent Boundary Layer," *Appl. Mech. Rev.*, **50**, pp. 689–729.
 [16] George, W. K., Wosnik, M., and Castillo, L., 1997, "Similarity Analysis for Forced Convection Thermal Boundary Layer," *10th International Symposium in Transport Phenomena in Thermal Science and Process Engineering*, Kyoto, Japan, Vol. 1, pp. 239–244.
 [17] Wang, X., and Castillo, L., 2003, "Asymptotic Solutions in Forced Convection Turbulent Boundary Layers," *J. Turbul.*, **4**, pp. 1–18.
 [18] Blackwell, B. F., 1972, "The Turbulent Boundary Layer on a Porous Plate: An Experimental Study of the Heat Transfer Behavior with Adverse Pressure Gradients," Ph.D. thesis, Stanford University, Palo Alto.
 [19] Reynolds, W. C., 1957, "Heat Transfer in the Turbulent Incompressible Boundary Layer with Constant and Variable Wall Temperature," Ph.D. thesis, Stanford University, Palo Alto.
 [20] Kong, H., Choi, H., and Lee, J., 2000, "Direct Numerical Simulation of Turbulent Thermal Boundary Layers," *Phys. Fluids*, **12**, pp. 2555–2568.
 [21] Schlichting, H., and Gersten, K., 2000, *Boundary Layer Theory*, Springer, New York.
 [22] Oberlack, M., 1996, "Symmetries in Turbulent Boundary Layer Flows," *Annual Research Briefs*, Center for Turbulence Research, Stanford University/NASA Ames, pp. 183–197.
 [23] Monin, A. S., and Yaglom, A. M., 1971, *Statistical Fluid Mechanics*, MIT, pp. 327–347.
 [24] Granville, P., 1976, "A Modified Law of the Wake for Turbulent Shear Layers," *ASME J. Fluids Eng.*, **98**, pp. 578–580.
 [25] Van Dyke, M., 1964, *Perturbation Methods in Fluid Mechanics*, Academic, New York.
 [26] White, F. M., 1974, *Viscous Fluid Flow*, 1st ed., McGraw-Hill, New York.
 [27] Kays, W. M., and Crawford, M. E., 1993, *Convective Heat and Mass Transfer*, 3rd ed. McGraw-Hill, New York.
 [28] Bell, D. M., and Ferziger, J. H., 1993, "Turbulent Boundary Layer DNS With Passive Scalars," *Near-Wall Turbulent Flows*, R. M. C. So, C. G. Speziale, and B. E. Launder, eds., Elsevier, Amsterdam, pp. 327–336.
 [29] Kays, W. M., 1994, "Turbulent Prandtl Number-Where Are We?," *ASME J. Heat Transfer*, **116**, pp. 284–295.
 [30] Succi, J., 2005, "Calculation of Turbulent Boundary Layers Using Equilibrium Thermal Wakes," *ASME J. Heat Transfer*, **127**, pp. 159–164.
 [31] Taylor, R. P., Love, P. H., Coleman, H. W., and Hosni, M. H., 1989, "The Effect of Step Changes in the Thermal Boundary Condition on Heat Transfer in the Incompressible Flat Plate Turbulent Boundary Layer," *Proceedings of the 1989 National Heat Transfer Conference*, Vol. 107, pp. 9–16.